Numerical Investigation of the Flow Within a Turbofan Lobed Mixer

P. Koutmos* and J. J. McGuirk†
Imperial College, London, England, United Kingdom
C. H. Priddin‡
Rolls-Royce plc, Derby, England, United Kingdom
and
M. N. Sodha§
Imperial College, London, England, United Kingdom

A computational procedure is described for the calculation of the flowfield within a multilobed turbofan mixer. The predictions have been obtained by using a finite-volume solution procedure for the three-dimensional elliptic equations of fluid flow extended to allow the modeling of flows within complex geometries. Turbulence is modeled using the two equation k-ϵ eddy viscosity model. Previous experimental investigations have shown that large scale secondary flows at exit from the lobes play a dominant role in the mixing process downstream of the lobe exit plane. The present work demonstrates the capability of the current method to predict the flow characteristics within the lobes and hence the formation of these secondary velocities. Finally, parametric studies of the effect of changes in the fan-side geometry are reported to investigate how these influence the flow structure, in particular the generation and amplification of the secondary flow patterns. The calculations provide useful information on the nature of the secondary flows and demonstrate how the procedure may be used to examine the likelihood of flow separation and the influence of the thickening of upstream boundary layers.

Nomenclature

A = cross-sectional area
$c_\mu, c_{\epsilon 1}, c_{\epsilon 2}$ = constants in k-ϵ turbulence model
k = turbulence kinetic energy
L = mixer length, = 320 mm
P = static pressure
PD = perpendicular distance from cell node to boundary
R = radius
U, V, W = mean velocities in cylindrical polar coordinates x, r, θ
$\overline{u_i u_j}$ = Reynolds stress tensor
x, r, θ = cylindrical polar coordinates
δ_{ij} = Kronecker delta, = 1 for $i = j$, = 0 for $i \neq j$
ϵ = turbulence energy dissipation rate
θ = circumferential coordinate in cylindrical polar system
θ_0 = angle of sector containing lobe: peak to trough, = 11.25 deg
μ_t = turbulent viscosity
ρ = density
$\sigma_k, \sigma_\epsilon$ = constants in k-ϵ turbulence model

Subscripts

i, j = indices of the tensorial notation

Superscripts

$-$ = mean value

Introduction

IN turbofan engines the use of lobed mixer geometries to reduce spatial nonuniformities in the velocity and temperature profiles between hot core and cold bypass flows is attractive in that it offers the potential of valuable gains in specific fuel consumption and thrust. If this is to be achieved in minimum length (to reduce additional pressure losses) and with the requirement of minimum weight, then the choice of an optimum geometry is crucial. Among the parameters to be determined by a mixer designer are the number of lobes, the lobe shape and degree of radial penetration, the plug and tailpipe angle and length, and the use of scarfing or scalloped lobes. The traditional approach relies on identifying an optimum combination of this large number of parameters through model scale and then selective full scale testing; this is, however, both expensive and time consuming. These difficulties have led to a number of investigations into the adequacy and applicability of numerical procedures based on computational fluid dynamic techniques for predicting the flowfield relevant to the above problem. The vast majority of this effort has restricted attention to the mixing duct itself, i.e., the region between the exit plane of the lobes and the exit plane of the tailpipe nozzle. Additionally, previous numerical procedures have mainly involved three-dimensional parabolic versions of the governing equations (e.g., Birch et al.[1] and Kreskovsky et al.[2]), which require only a single forward marching sweep through the mixing duct downstream of the lobe exit plane. These predictions have by and large been very encouraging when compared with the available measurements,[3,4] although some criticism of the validity in such flows of a once-through marching procedure has been expressed by Barton and Birch[5] and McGuirk and Whitelaw.[6] Far more significantly, all of the published investigations on mixer calculations have emphasized the absolute necessity, within the calculation framework adopted, for a precise specification of the three-dimensional velocity field at the inlet to the calculation region (i.e., at the

Received Sept. 27, 1989; revision received March 5, 1990.

*Fluids Section, Department of Mechanical Engineering; currently, Lecturer, Department of Mechanical Engineering, University of Patras, Greece.
†Fluids Section, Department of Mechanical Engineering; currently, Professor of Aerodynamics, Department of Transport Technology, Loughborough University, Leicestershire LEII 3TU, UK.
‡Manager, Combustion Methods.
§Research Assistant, Department of Chemical Engineering and Chemical Technology.

exit plane of the lobes[2,3]). Only when such inlet conditions were adequately specified could the calculation procedures deliver reasonable simulations of experimental data.

This conclusion is particularly significant and is strongly supported in light of the detailed experimental investigation of Paterson[7]; this demonstrated the complexity of the velocity field created within the lobes and the strong dominance of the lobe generated secondary flows over the nozzle mixing process. This implies that the computational approaches adopted to date are dependent on the availability of suitable experimental data (e.g., Paterson[7]) for interpolation as inlet boundary conditions for the mixing duct calculation.

An initial attempt to model the secondary flows within the lobe geometry itself (and thus to provide inlet conditions for the spatial marching mixer codes) has been reported recently by Barber et al.[8,9] These authors used inviscid concepts to predict the generation of the array of streamwise vortices at the lobe exit. A potential flow analysis, based on a zonal approach, was developed; a separation of variables technique was adopted so that a quasi-three-dimensional procedure resulted and calculations were performed for a series of axisymmetric problems. Not only was the analysis restricted to slender mixer lobes (whose change in radius is small compared to their length), but it is only applicable if the flow remains attached on the lobe surface. Even then the inviscid analysis would need to be combined with a lobe boundary-layer calculation to provide truly representative starting conditions for the marching viscous calculations. Clearly a potential flow model of the lobe flow is valuable in describing the gross features of the periodic distributions of circulation at the mixing plane, but it is unlikely that the model will provide detailed descriptions of the exit velocities or the minor horseshoe like vortices that occur in some types of mixers.[3] Further, this type of approach currently precludes studies of the effect of inlet conditions on mixer performance (e.g., increased turbulence and thickening of the upstream boundary layers).

The aim of the present work is to extend the capability of a current, standard finite-volume technique (including viscous effects) to model the flows within arbitrary three-dimensional geometries so that the analysis can be extended to include the lobes themselves. The calculations are made possible by using a general method for treating complex geometries within finite-volume techniques based on simple (e.g., Cartesian or cylindrical polar) coordinate systems.[10,11] This type of approach has already been applied to the calculation of flow within complex gas turbine combustor configurations.[12] The calculations described are concerned primarily with the prediction of the flow within the lobes; at present only coplanar mixers without scarfing or scallops are considered. The capability of the method and the plausibility of the predictions are examined with a view to future applications of this method to provide a more accurate and flexible analysis of the flow in the mixer nozzle.

Mathematical Model

The calculations presented here have been obtained by solving the full three-dimensional elliptic forms of the equations for conservation of mass and momentum in time-averaged form; using Cartesian tensor notation for convenience, these may be written as

$$\frac{\partial}{\partial x_i}(\rho U_i) = 0$$

$$\frac{\partial}{\partial x_j}(\rho U_i U_j) = -\frac{\partial \bar{P}}{\partial x_i} - \frac{\partial}{\partial x_j}(\rho \overline{u_i u_j})$$

Uppercase letters represent time-mean quantities and lowercase fluctuating components; the $\rho \overline{u_i u_j}$ are the turbulent Reynolds stresses. In the present calculations, solutions are sought only for the flow within the lobes themselves; the downstream development in the mixing duct is the subject of a separate study.[13] Hence, the exit plane for the current calculations is the exit plane of the lobes themselves, here assumed coplanar (i.e., perpendicular to the engine centerline). Accordingly, the bypass and turbine streams were considered isothermal and physically separated with relatively low Mach numbers; thus, density fluctuations are considered negligible, and the density is assumed constant throughout each of the streams. The problem is just reduced to solving for the velocity and pressure field on each side of the lobe surface. The turbulent momentum fluxes are here approximated via the high Reynolds number version of the two-equation k-ϵ turbulence model introduced by Jones and Launder.[14] The Reynolds stress is linearly related to the mean rate of strain via a scalar turbulent viscosity:

$$-\rho \overline{u_i u_j} = \mu_t \left(\frac{\partial U_i}{\partial x_j} + \frac{\partial U_j}{\partial x_i} \right) - \frac{2}{3} \delta_{ij} \rho k$$

and the turbulent viscosity is expressed as

$$\mu_t = C_\mu \rho \frac{k^2}{\epsilon}$$

where the values of k and ϵ are obtained from solution of the transport equations:

$$\frac{\partial}{\partial x_j}(\rho U_j k) = \frac{\partial}{\partial x_j}\left(\frac{\mu_t}{\sigma_k} \frac{\partial k}{\partial x_j} \right) - \rho \overline{u_i u_j} \frac{\partial U_i}{\partial x_j} - \rho \epsilon$$

$$\frac{\partial}{\partial x_j}(\rho U_j \epsilon) = \frac{\partial}{\partial x_j}\left(\frac{\mu_t}{\sigma_\epsilon} \frac{\partial \epsilon}{\partial x_j} \right) - C_{\epsilon 1} \frac{\epsilon}{k} \rho \overline{u_i u_j} \frac{\partial U_i}{\partial x_j} - C_{\epsilon 2} \rho \frac{\epsilon^2}{k}$$

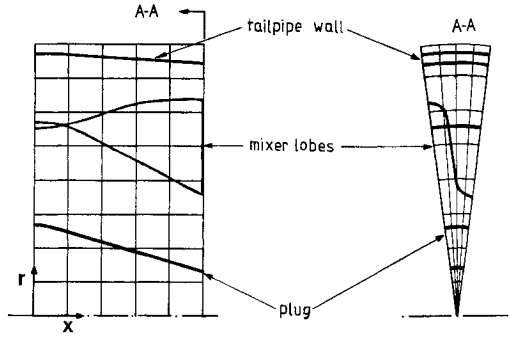

Fig. 1 Typical mixer geometry embedded within cylindrical polar grid.

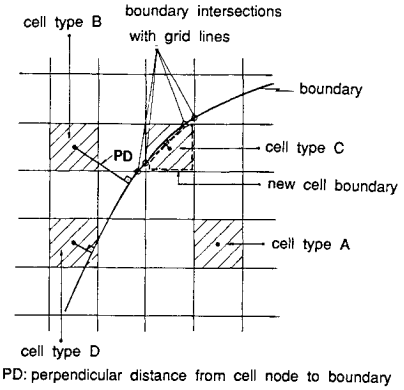

Fig. 2a Boundary cell classification.

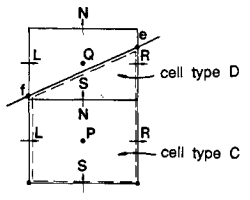

Fig. 2b Partially external cell treatment.

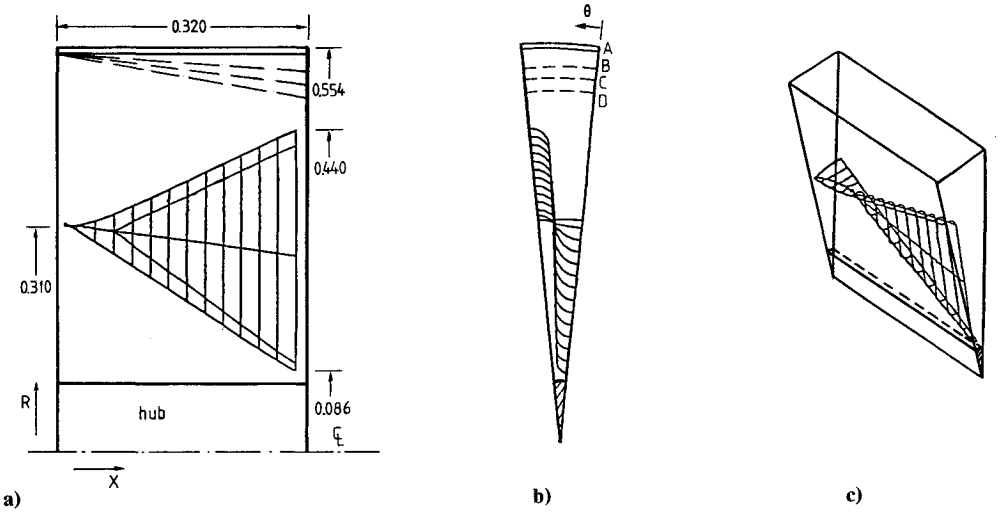

Fig. 3 Lobed mixer geometry: a) side view; b) looking upstream; c) 45-deg view.

The model contains five empirical constants, which are assigned the following values, found to give good agreement in a wide range of two-dimensional shear flows[15]:

$$C_\mu = 0.09, \quad C_{\epsilon 1} = 1.44, \quad C_{\epsilon 2} = 1.92, \quad \sigma_k = 1.0, \quad \sigma_\epsilon = 1$$

Such a simple turbulence model might be thought inappropriate given the complexity of the present flow. However, the same model was used by Kreskovsky et al.,[2] who found, at least for the mixing duct flow, that calculations of the secondary flow development were fairly insensitive to the turbulence model, apart from the fine scale details.

The solution of the above six steady-flow, three-dimensional coupled partial differential equations were obtained using a finite-volume scheme. The formulation comprises a linearized implicit conservative scheme using central differencing except in regions where mean flow convective fluxes dominate diffusive processes in which case donor cell differencing is used. The method is formulated in terms of velocity and pressure using a staggered grid arrangement. The pressure velocity coupling is handled via the standard SIMPLE pressure correction algorithm.[16] One advantage of pressure correction methods is that they guarantee that mass continuity is satisfied at each point and therefore on each plane of the solution domain; the convergence criterion used here is that the sum of all mass source errors must be less than 0.01% of the flow through the duct. The method has been used in several three-dimensional recirculating flow problems, including a study of primary zone flow patterns in a can-type gas turbine combustor.[12] The algorithm is coded such that either Cartesian or cylindrical polar coordinate systems may be used.

For the calculation of flows within three-dimensional geometries with arbitrary boundaries, two alternative approaches are available. The use of a boundary conforming mesh (orthogonal or nonorthogonal) and transformed versions of the governing equations is one possibility under active development at the present time for several internal flow problems. Although very promising for the present application, the complexity of the lobe geometry perhaps implies that such methods require further development before being applied to mixer flows. At the very least, no attempts have yet been made to apply such methods to lobe flows to the authors' knowledge. A second alternative is to retain the simple coordinate system and to formulate special treatment for the boundary cells. This is the technique adopted here and indeed has also been used in the only other attempt to calculate the flow within the lobes.[8,9] As pointed out by these authors, the complexity of the boundary/mesh intersection treatment when a simple coordinate description is retained is in effect equivalent to the complexity introduced by the mesh generation, equation transformation, and algorithm modifications required in the boundary conforming approach. One advantage of the simple coordinate approach in the present problem is that, as shown below, exactly the same mesh may be used for both fan-side and core-flow streams.

Accordingly, for all calculations discussed in the following, the cylindrical polar version of the governing equations has been used and an x-r-θ mesh generated, which encompasses the whole lobe section, as sketched in Fig. 1. As seen in this figure, the solid boundaries intersect the mesh at irregular positions resulting in irregular shapes and sizes of boundary cells. The first problem is to identify these boundary cells and the second is to formulate a new finite-volume equation for these cells depending on their shape and position relative to the solid surface.

The precise geometry of the solid boundaries is specified by first providing the intersections of the chosen grid lines with the boundary surface. The surface description of typical lobe shapes may be given in an algebraic form by dividing the surface into a series of sections perpendicular to the engine centerline, each of which may be described by a combination of straight lines and circular arc segments. Any level of interpolation may be used in between these specified cuts through the lobes, and the intersections of any grid line with the numerically discretized surface may be easily calculated as shown in Fig. 2a. Four types of cell volume are then defined using identifying tags attached to each cell vertex according to whether it lies inside or outside the flow domain as specified from the nearest intersection points: 1) cell type A: fully internal, all corners inside the flow region; 2) cell type B: fully external, all corners outside; 3) cell type C: boundary cell, intersected by solid boundary with central node inside flow; and 4) cell type D: boundary cell, intersected by solid boundary with central node outside flow. This identification process must of course be carried out for all of the staggered mesh systems used. For each cell type, appropriate actions may then be taken. For type A, no changes to the code are required. For type B, usually zero values are fixed at the grid nodes for all dependent variables. It should be pointed out here that type B cells constitute not only cells outside the tailpipe wall or inside the plug, but, for convenience, the core and fan flows have been calculated separately on the same mesh. Thus, when calculating the fan side, all points at lower radii than the lobe surface are treated as type B; similarly, for the core-flow calculation, points in the fan side are treated as external. A method for interacting the two flows has been developed,[13] and this point is returned to again later.

For boundary cells of type C, the correct cell wall fluxes are calculated using geometric information deduced from a locally planar approximation to the part of the boundary surface

contained within the cell (equivalent to a piecewise linear fit to a curve in two dimensions). The intersection points are used to calculate the proportion of each of the six cell face areas lying inside the flow domain, the perpendicular distance from the grid node to the wall, the local direction cosines of the boundary normal, and the area of the boundary contained within the cell. These latter pieces of information are required for the implementation of the usual wall function approach[15] to allow the inclusion of the wall shear stress in the finite-volume formulation for the boundary cells. Finally, for type D cells, to ensure that no portions of the flow domain are "lost," the internal portion of the cell is added on to the nearest cell possessing an internal node to give rise to a new extended type C cell as shown by the dashed line in Fig. 2b. If more than one possible add on direction is available, the internal cell with the largest contact face area is chosen. Subsequent to these actions, cell type D is treated as a fully external cell.

In this manner, the location of the solid surface is communicated to the cylindrical polar mesh, within the precision of a piecewise planar approximation, which can obviously be improved by mesh refinement. In all other respects, the solution algorithm remains unchanged from its standard version.

Modeled Geometry and Boundary Conditions

To demonstrate the ability of the method just described to calculate flow through mixer lobes, a model problem has been devised. A 16-lobed mixer is considered, but geometric symmetry and periodic repeatability require a solution only for a sector formed by the 11.25-deg slice comprising one-half of a lobe, as shown in Fig. 3, extending from a lobe peak to a lobe trough with symmetry boundary conditions along the edge planes of the sector. Figure 3a also gives the assumed dimensions of the mixer, and it should be pointed out that these do *not* correspond to the slender approximation mentioned earlier, underlining the generality of the current method. For simplicity a constant radius plug has been chosen since emphasis is here placed on the lobe shape. In most calculations that follow, a grid consisting of $20\times8\times11$ (r,θ,x) nodes represented the cylindrical polar calculation domain. This corresponds to a coarse mesh for such a complex geometry, complex flow problem. This was deemed sufficient, since the emphasis of the present investigation was to demonstrate the feasibility of calculating the flow within the lobes. In a real problem, a finer mesh would of course be used. To illustrate that this level of mesh coarseness is still capable of resolving the main flow features, Fig. 4 is provided. This shows (for a different but similar lobe/plug geometry to that described above) axial velocity (Fig. 4a) and radial velocity (Fig. 4b) profiles at three stations through the mixer for two grids, a coarse mesh ($20\times8\times11$) and a mesh refined by a factor of 2 in each coordinate direction ($40\times16\times22$). Although certain small scale features near the walls are not picked up in the coarse mesh, the overall shape and level of the profiles are very similar on both peak and trough planes. In particular, the important V component representing the secondary flow is similar in magnitude and shape in both meshes. Barber et al.[8,9] do not quote how many axial stations they used over the lobe length, but Kreskovsky et al.[2] used only 20 stations over the whole mixing duct length. A nonuniform grid distribution was set up for optimum resolution of the lobe variation from inlet to outlet. As mentioned previously, the same grid was used for both the fan and core-flow predictions, which were performed independently of each other, however. This offers the advantage that only one set of intersections of the lobe surface with the grid is required for each calculation (the lobe is assumed to be thin).

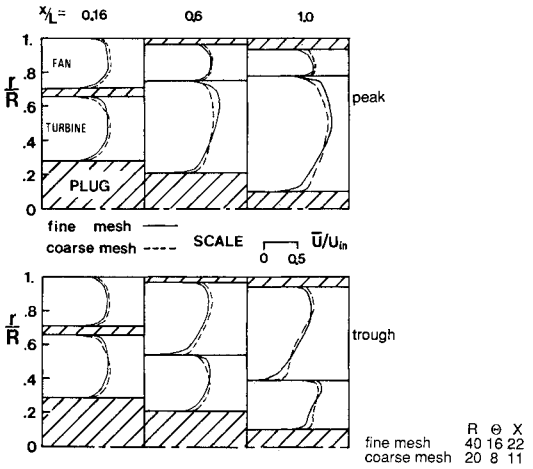

Fig. 4a Grid refinement tests, axial velocity profiles.

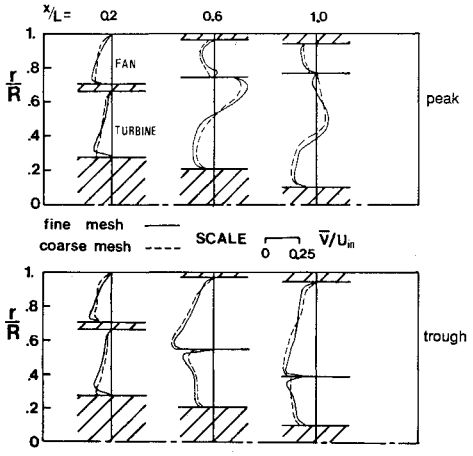

Fig. 4b Grid refinement tests, radial velocity profiles.

The mass flows for the fan and core sides were 53.4 kg/s and 10.3 kg/s with corresponding inlet air axial velocities of 80 and 95 m/s. At the upstream boundary of the calculation, the axial velocity profile was taken to be similar to that of fully developed annulus flow, and the V and W components were assumed zero. Levels of turbulence kinetic energy were chosen as 3 and 5% for the fan and turbine streams, respectively. These values are similar to those used in a number of computational investigations of mixer flows (e.g., Birch et al.[1] and Anderson and Povinelli[3]). Boundary values for energy dissipation rate were calculated using an assumption of a length scale proportional to the appropriate inlet annular height.

This completes the prescription of the inlet conditions. For boundary conditions on all solid surfaces, as mentioned previously, wall functions have been used; these calculate the value of the local wall shear stress and near wall velocity gradients assuming that the near wall velocity lies in the fully turbulent logarithmic wall law region. At the outlet of the lobes, for the present calculations, a simple zero gradient extrapolation boundary condition has been used. This implies that the fan and turbine streams are being considered as *separate* duct flows with prescribed upstream conditions. When the lobe flow is coupled with the mixing duct flow, it is clear that some compatibility conditions must be used to ensure the lobe trailing edge region is calculated properly. Koutmos and McGuirk[13] describe how an iterative procedure to ensure that the flows on both sides of the lobes exit to the *same* static pressure field may be used to satisfy the fan/turbine stream compatibility. The current paper concentrates only on the lobe flow, and so the compatibility has not yet been enforced, and this can cause an error, although results shown later indicate that this is small. The present calculations may be viewed as the first pass of an overall iteration loop; further passes through the system would enforce the trailing edge Kutta condition and reduce the present small error even further. In the case of a complete mixer/downstream duct calculation,

Table 1 Planes for streakline pictures

Plane a	x-r	$\theta = 0$ deg	through lobe trough
Plane b	x-r	$\theta = 6$ deg	midway between lobe trough and peak
Plane c	x-r	$\theta = 11.25$ deg	through lobe peak
Plane d	r-θ	$x/L = 0.2$[a]	
Plane e	r-θ	$x/L = 0.52$[a]	
Plane f	r-θ	$x/L = 0.75$[a]	
Plane g	r-θ	$x/L = 1.0$[a]	

[a]Transverse section down the mixer length.

power addition would be handled by specifying different levels of inlet total pressure, calculated from a quasi-one-dimensional analysis expanding both streams to a single downstream static pressure, in a manner similar to that described by Barber et al.[8,9]

Parametric studies have also been made with different outer wall casing positions in order to investigate different fan-side area ratios. This is particularly important since it is usually in the bypass side that flow detachment may occur. Five runs were made with area ratios (A_{outlet}/A_{inlet}) of 0.81, 0.88, 0.96, and 1.15, which corresponded to outer wall positions D, C, B, and A as given in Fig. 3. The core side remained unaltered with an area ratio of 0.7. Results are presented in terms of streakline plots to provide an overall qualitative assessment of the predicted flow patterns. This computational flow visualization is achieved by tracking weightless particles through the predicted velocity field on a given two-dimensional plane for a finite time (tracking time) and represents a quick, accurate method of illustrating the predicted changes in flow patterns for the various fan area ratios. The positions at which these plots were obtained are given in Table 1.

In order to enable better flow visualization in the streakline plots, the circumferential direction has been enlarged by a factor of 5. For r-θ planes, streaklines have been obtained with a tracking time of 2.5 ms, three times that used for the axial planes. Note also that the r-θ planes are shown from the viewpoint of someone looking downstream in the lobes.

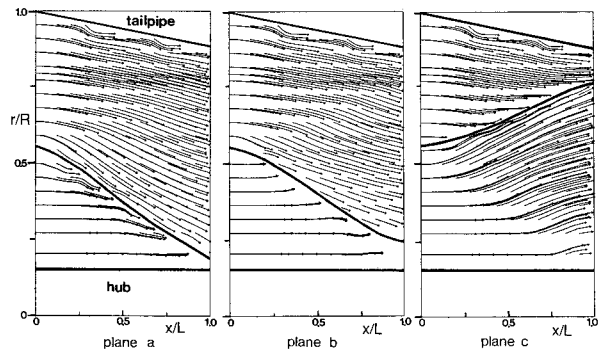

Fig. 5 Predicted flow patterns for area ratio of 0.81: axial planes.

Results and Discussion

Streaklines of the predicted velocity fields in the axial planes through the trough, midway between peak and trough, and through the peak of the lobe are shown in Fig. 5 for a fan-side area ratio of 0.81. In the fan stream, the plots suggest a rapid growth of inward radial flow over almost the whole extent of the flow domain. In the vicinity of the trough (plane a), the streaklines are nearly aligned with the slope of the lobe contour as would be expected from the absence of flow detachment. The slightly undulating flow patterns in the vicinity of the walls, particularly near the outer tailpipe walls, is caused by a problem associated with the rather coarse representation in the present mesh of the outer wall and the treatment of the pressure correction equation for cells that contain only one surrounding velocity node that is internal to the flow. An alternative practice has been developed to overcome this problem, and later calculations[13] do not show this defect; the practice does not, however, invalidate any of the principal conclusions of the present work. The ratio of radial to axial velocity at exit is therefore close to the tangent of the lobe penetration angle (35 deg). In contrast to this, the core flow is accelerating and remains fairly uniform away from the lobe surface. Noticeable radial velocities occur only in the immediate vicinity of the lobe peak as indicated by streaklines parallel to the engine centerline near the inlet and the hub (Fig. 5, planes a, b, c). The developing cross-plane flows are seen better in the azimuthal direction plots depicted in Fig. 6. Their onset is evident as early as $x/L = 0.2$ (plane d), where the much stronger radial flows generated in the fan side are again visible. The beginnings of a streamwise vortex element centered on the sloping walls of the lobe can also be clearly identified. The orientation and distortion of the streaklines (planes d, e, f, g) suggest momentum transfer from the azimuthal to the radial direction and indicate the strong effect of the lobe geometry on the generation of these pressure driven secondary velocities.

By the mixer exit plane ($x/L = 1$), the anticlockwise rotating vortex (looking downstream) is restricted to the neighborhood of the top corners of the lobe peak; the main transverse velocities are radial and of opposite direction on each side of the dividing lobe surface. This implies that, for the present geometry, the dominant mode of secondary velocity is the turning or flap vorticity as described by Povinelli and Anderson.[4] Radial velocities in the bypass stream, at this position, were 35% of the inlet axial velocity, whereas in the turbine stream, they comprised about 30% of the respective inlet axial velocity.

The rotation of the vortex predicted near the lobe peak in the outer (fan) stream is in a sense opposite to the horseshoe vortex mechanism observed by Povinelli and Anderson.[4] However, vortices in this location and rotating in this sense have been observed[17] for rectangular shaped lobes, and, as seen in Fig. 6b, the current lobe shape follows this shape quite closely. No evidence exists for the small passage vorticity postulated by Povinelli and Anderson,[4] although the large penetration and small gap between centerbody and lobe trough are exactly those circumstances in which it is believed such passage vortic-

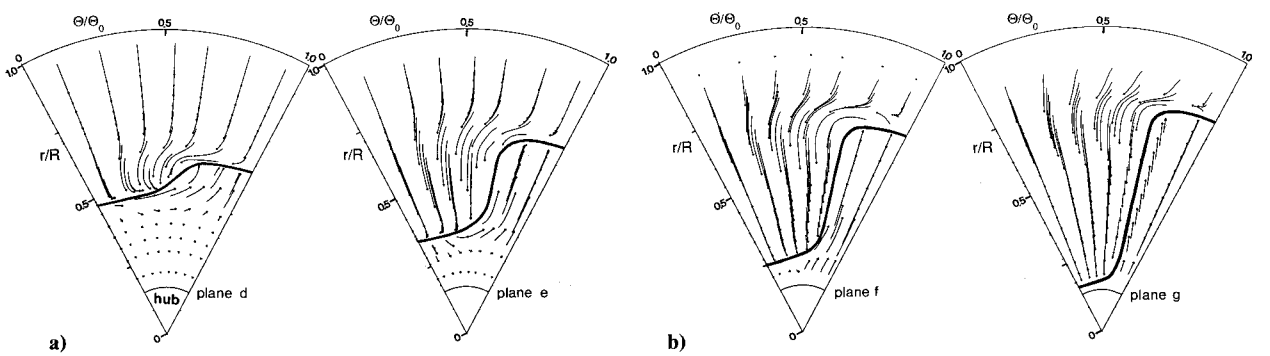

Fig. 6 Predicted flow patterns for area ratio of 0.81: a) azimuthal planes d and e; b) azimuthal planes f and g.

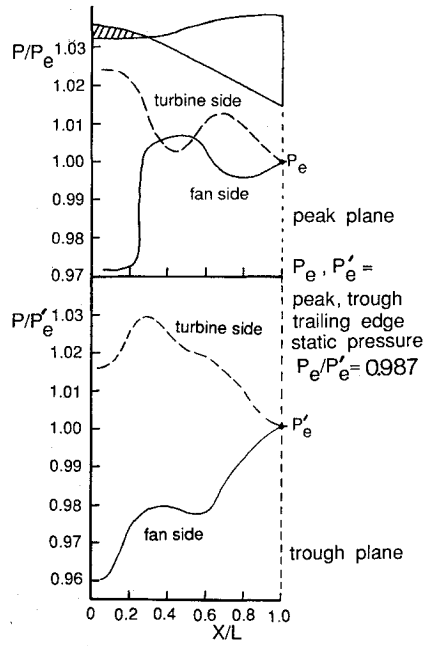

Fig. 7 Wall static pressure distributions on lobe peak and trough, fan side and turbine side.

ity mechanisms are strongest. Perhaps insufficient grid resolution prevented this in the present calculations.

The aforementioned figures indicate the nature of the flowfield within the lobes and the rapid growth of the secondary velocities as the lobe geometry develops. This flow pattern induces significant static pressure gradients in the flow as indicated in Fig. 7 for two sections passing through a lobe peak and a lobe trough. It is very noticeable now large variations in static pressure begin to enter as soon as the lobe breaks away from the upstream axisymmetric shape; very similar observations were made by Barber et al.[8,9]

The formation of the secondary velocities has also been investigated as a function of the fan-side area ratio. It is in the bypass stream that deceleration and further diffusion of the flow is attempted, and this may sometimes lead to local separation on the lobe surface. Figures 8, 9, and 10 depict the predicted flow patterns for three exit areas different from that discussed above, obtained by progressively inclining the outer casing radially outwards (Fig. 3a), All other inflow boundary conditions remained the same. At an area ratio of 0.88, the predicted flow remained attached in the axial direction (Fig. 8a), whereas in the azimuthal direction, the streakline plots (Fig. 8b) indicate a small flow detachment near the lobe trough. Otherwise the velocity field is quite simlar to the 0.81 area ratio case. The inward radial velocities at the exit plane were, however, reduced to 17% of the inlet axial velocity. As the area ratio is progressively increased to 0.96 (Fig. 9) and then to 1.15 (Fig. 10), a recirculation appears in the axial direction near the trough on the fan side. Not unexpectedly, the strength of the flow reversal becomes more pronounced as the area ratio increases. The azimuthal flow reversal also grows in strength so that quite large *outward* flows are obtained near the lobe surface. Both these effects allow the fan flow to pass undeflected through the duct, so that average radial velocities are progressively decreased with the most significant reduction occurring near the trough of the fan. At these higher area ratios, a vortex originating halfway through the lobe length was established on the azimuthal planes. Once again, the origin of this vortex does not seem to be of the horseshoe type, and the direction of the rotation and size of the vortex confirm this. The predictions rather suggest this to be the result of large scale separation on the azimuthal plane as the fan flow turns and washes around the lobe peak.

In considering the analysis of these results, it should be restated that so far the flows in the core and bypass streams have been calculated separately, and no attempt has been made to impose the compatibility which must be enforced as soon as the wall separating the two streams ends and mixing begins. Both streams should flow through the lobes towards the same pressure field at the mixer exit plane, and this may alter the flow upstream.[13] It is likely, however, that when no appreciable separation is present at the mixer exit, the results are qualitatively acceptable.

Turbulence levels are generally thought to play a rather insignificant role in the generation and development of pressure driven (skew induced) secondary flows; this seems to be supported by the turbulence model tests performed by Anderson and Povinelli[3] for the downstream mixing duct flow. In the present predictions, the mixing plane turbulence levels were up to seven times the inlet values, and this suggests considerable turbulence generation in the developing flows. Figures 11a

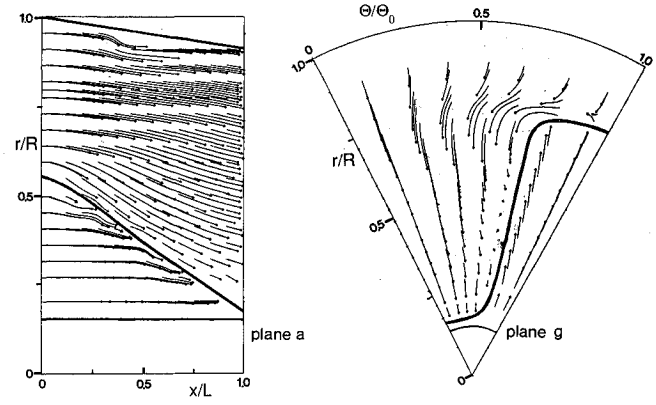

Fig. 8 Predicted flow patterns for area ratio of 0.88.

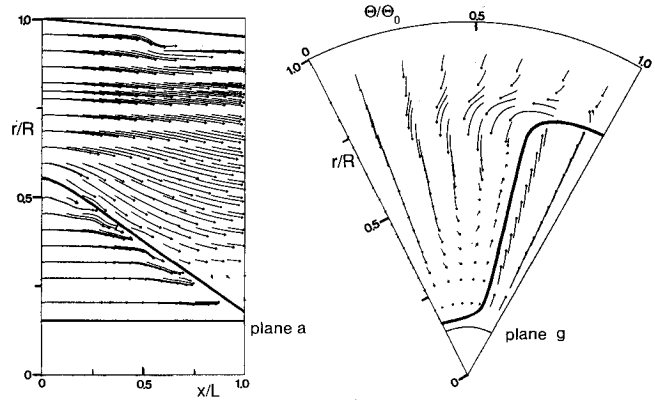

Fig. 9 Predicted flow patterns for area ratio of 0.96.

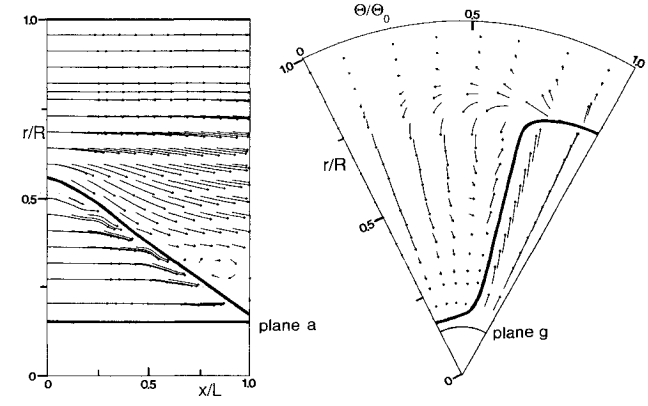

Fig. 10 Predicted flow patterns for area ratio of 1.15.

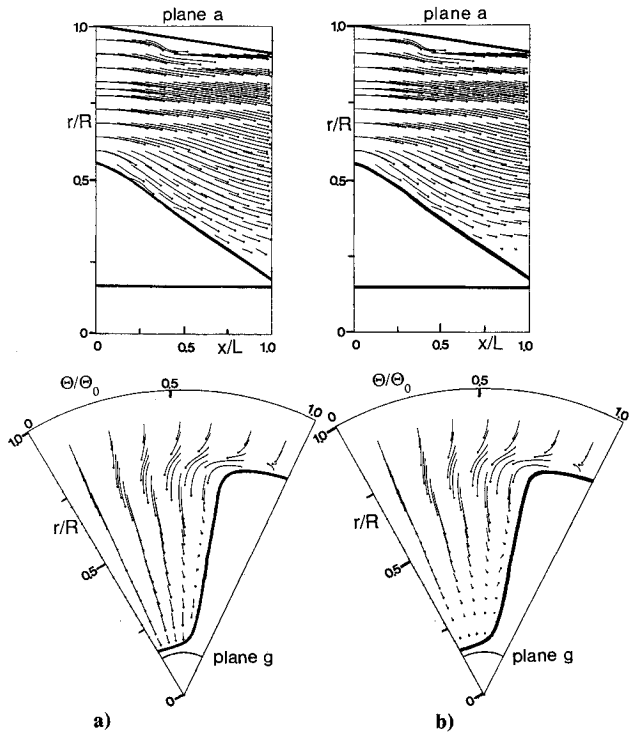

Fig. 11 Investigation of inlet turbulence levels effect on flow pattern for area ratio of 0.88: a) inlet turbulence at 3%; b) inlet turbulence at 10%.

and 11b show the predicted flow patterns for two different inlet turbulence levels of 3% (Fig. 11a) and 10% (Fig. 11b) with a fan-side area ratio of 0.88. The increase in turbulence energy speeds up the boundary-layer growth on the lobe surface (Fig. 11b, plane a) and decreases the trough axial velocities. In accord with the trends discussed previously, the change is then more apparent in the azimuthal planes where the cross-plane vortex strengthens and the inward radial velocities decrease. It seems that the thickened boundary layer in the second case is almost on the point of separation (see Fig. 11b, plane a); this ability even on a coarse mesh to resolve small scale localized incipient separation effects caused by the upstream boundary layer changes is most encouraging since, from a design viewpoint, this is an important feature to be avoided for a good mixer performance.

Summary

A finite-volume procedure capable of calculating the flow within complex three-dimensional geometries has been further developed and used to compute the aerodynamic flow within a turbofan lobed mixer. The calculated results suggested the capability of the method in predicting the streamwise vorticity generated by the radial deflection of the fan and turbine streams within and at the exit from the lobes. These all important exit radial flows of opposite direction induce the onset of an array of vortex cells, which are known to control mixing in the downstream duct and are an essential input for the accurate prediction of this region. The present parametric investigation also indicated the usefulness of the analysis as a research or design tool to ascertain what type of inflow conditions or mixer geometry lead to desirable mixer performance. The extension of the method to allow coupling between the present lobe flow calculations and the mixing duct calculations is currently underway.[13] Finally, to reinforce the qualitative study reported here, a thorough testing of the current method against experimental validation data[18] is also in hand.

Acknowledgments

The work reported here has been supported by Rolls-Royce plc. The authors would like to acknowledge their gratitude for this support and the many useful discussions with staff of the Powerplant Technology section at Rolls-Royce (Derby).

References

[1]Birch, S. F., Paynter, G. C., Spalding, D. B., and Tatchell, D. G., "Numerical Modelling of Three Dimensional Flows in Turbofan Engine Exhaust Nozzles," *Journal of Aircraft,* Vol. 15, 1978, p. 489.

[2]Kreskovsky, J. P., Briley, W. R., and McDonald, H., "Investigation of Mixing in a Turbofan Exhaust Duct. Part 1: Analysis and Computational Procedure," *AIAA Journal,* Vol. 22, No. 3, 1984, p. 374.

[3]Anderson, B. H., and Povinelli, L. A., "Factors Which Influence the Behaviour of Turbofan Forced Mixer Nozzles," NASA TM-81668, 1981.

[4]Povinelli, L. A., and Anderson, B. H., "Investigation of Mixing in a Turbofan Exhaust Duct. Part II: Computer Code Application and Verification," *AIAA Journal,* Vol. 22, No. 4, 1984, p. 518.

[5]Barton, J. M., and Birch, S. F., "Numerical Modelling of Three Dimensional Turbulent Jet Flows," AIAA Paper 80-0008, 1980.

[6]McGuirk, J. J., and Whitelaw, J. H., "Internal Flows of Relevance to Gas Turbines," *Computation of Internal Flows: Methods and Applications,* ASME Fluids Engineering Division Publication, Vol. 14, edited by P. M. Sockol and K. N. Ghia, New York, 1984, p. 37.

[7]Paterson, R. W., "Turbofan Mixer Nozzle Flow Field—A Benchmark Experimental Study," *ASME Journal of Engineering for Gas Turbines and Power,* Vol. 106, 1984, p. 692.

[8]Barber, T. J., Muller, G. L., Ramsey, S. M., and Murman, E. M., "Three Dimensional Inviscid Flow in Mixers, Part I: Mixer Analysis Using a Cartesian Grid," *Journal of Propulsion and Power,* Vol. 2, No. 3, 1986, p. 275.

[9]Barber, T. J., Muller, G. L., Ramsey, S. M., and Murman, E. M., "Three Dimensional Inviscid Flow in Mixers, Part II: Analysis of Turbofan Forced Mixers," *Journal of Propulsion and Power,* Vol. 2, No. 4, 1986, p. 339.

[10]McGuirk, J. J., and Spalding, D. B., "The Treatment in the Three-Dimensional Boundary Layer Program of Walls Which do not Pass Through Grid Nodes," Mechanical Engineering Dept., Imperial College, London, Rept. HTS/73/13, 1973.

[11]Priddin, C. H., "A Version of PACE with Arbitrary Boundary Capability," Rolls-Royce Ltd., Derby, Internal Rept. CRR-89391, 1979.

[12]Koutmos, P., "An Isothermal Study of Gas Turbine Combustor Flows," Ph.D. Thesis, Univ. of London, London, 1985.

[13]Koutmos, P., and McGuirk, J. J., "Turbofan Forced Mixer/Nozzle Temperature and Flow Field Modelling," *International Journal of Heat and Mass Transfer,* Vol. 32, No. 6, 1989, p. 1141.

[14]Jones, W. P., and Launder, B. E., "The Prediction of Laminarisation with a Two Equation Model of Turbulence," *International Journal of Heat and Mass Transfer,* Vol. 15, 1972, p. 301.

[15]Launder, B. E., and Spalding, D. B., "The Numerical Computation of Turbulent Flow," *Computer Methods in Applied Mechanics and Engineering,* Vol. 3, 1974, p. 269.

[16]Patankar, S. V., *Numerical Heat Transfer and Fluid Flow,* Hemisphere, Washington, DC, 1981.

[17]Paterson, R. W., "Turbofan Forced Mixer-Nozzle Internal Flow Field, Vol. 1—A Benchmark Experimental Study," NASA CR 3492, 1982.

[18]Koutmos, P., and McGuirk, J. J., "Isothermal Velocity and Turbulence Measurements Downstream of a Model Multilobed Mixer," *Experiments in Fluids,* Vol. 8, 1989, p. 183.